Peer-Reviewed Article

Virtual Indicative Broadband over Power Lines Topologies for Respective Subclasses by Adjusting Channel Attenuation Statistical Distribution Parameters of Statistical Hybrid Models (Class Maps) – Part 1: Theory

Athanasios G. Lazaropoulos[*]

School of Electrical and Computer Engineering / National Technical University of Athens / 9 Iroon Polytechniou Street / Zografou, GR 15780

Based on a set of indicative overhead and underground medium voltage broadband over power lines (OV and UN MV BPL) topologies, initial statistical hybrid model (iSHM) and modified statistical hybrid model (mSHM) are statistical channel models suitable for the distribution BPL networks. Both iSHM and mSHM statistically process channel attenuation and capacity values of assumed indicative OV and UN MV BPL topologies by exploiting channel attenuation statistical distributions (CASDs). iSHM exploits a set of well-known CASDs (*i.e.*, Gaussian, Lognormal, Wald, Weibull and Gumbel CASDs) while mSHM exploits the Empirical CASD. Each indicative OV and UN MV BPL topology acts as the representative one of a respective OV and UN MV BPL topology class (*i.e.,* rural, suburban, urban and aggravated urban class) that consists of a number of respective statistically equivalent OV and UN MV BPL topologies. The contribution of this paper is the theoretical framework presentation of the creation of new virtual indicative OV and UN MV BPL topologies by appropriately adjusting the parameters of iSHM and mSHM CASDs. These new virtual indicative OV and UN MV BPL topologies will enrich the respective today's OV and UN MV BPL topology classes with respective OV and UN MV BPL topology subclasses while each subclass will be enriched by a number of respective statistically equivalent OV and UN MV BPL topologies. The procedure of defining new virtual distribution BPL topologies by applying iSHM and mSHM will allow a better capacity study of OV and UN MV BPL topology classes. Apart from the definition procedure of the virtual indicative OV MV and UN MV BPL topologies and their respective virtual subclasses by adjusting CASD parameters of iSHM and mSHM, the contribution of this paper is the class map that analytically describes the taxonomy of distribution BPL topology classes and subclasses.

1. Introduction

The today's traditional power grid is evolving to an intelligent IP-based communications network enhanced with a plethora of broadband applications, widely referred to as smart grid [1]-[13]. Actually, smart grid can support two types of flows; say, a two-way power and a two-way information flow [14]-[16]. As the two-way power flow is concerned, apart from the traditional power flow from power generators to the customers, there is the power that is generated by the customers and be injected back into the power grid. As the two-way information flow is concerned, the proposed broadband applications can help either power utilities to monitor, meter, control and provide valuable real-time detailed information on actual operation of the power grid or customers to control dynamic power flows and meet more profitably their power demands. Among the available communications solutions that can support this two-way information flow of smart grid is the Broadband over Power Lines (BPL) technology that can play important role since it may support an electronic communications channel (*i.e.*, BPL channel) upon the already installed wired power grid infrastructure and, at the same time, interconnect with other already installed communications solutions of the smart grid through its wireline/wireless interfaces [3], [17]-[28].

Dealing with the BPL statistical channel modeling, the initial statistical hybrid model (iSHM) has been proposed in [17, 18], while the modified statistical hybrid model (mSHM) has been proposed in [29]. Both models consist of six phases (*i.e.*, Phase A-F) while their core is the deterministic hybrid model of Phase B that has extensively been validated in transmission and distribution BPL networks and comprises two interconnected submodules, namely: (i) the bottom-up approach module; and (ii) the top-down approach module [4], [23]-[27], [30]-[34]. The common input data basis is the consideration of a set of indicative distribution BPL topologies that acts as the representative topologies of a set of respective distribution BPL topology classes –*i.e.*, rural, suburban, urban and aggravated urban classes– where each distribution BPL topology class is filled with statistically equivalent BPL topologies [17], [18], [29]. The result of iSHM and mSHM is the capacity range of each distribution BPL topology class for given operation frequency range, power grid type, injected power spectral density (IPSD) limits, noise level, coupling scheme and channel attenuation statistical distribution (CASD). As the CASDs are concerned, iSHM applies five well-known CASDs of the communications literature, say, Gaussian, Lognormal, Wald, Weibull and Gumbel ones [17, 18], while mSHM applies the Empirical CASD [29]. The selection of a CASD plays a critical role during the capacity range computation of each distribution BPL topology class since it mainly affects the results of the random number generator module (Phase D of iSHM and mSHM) through the maximum likelihood estimators (MLE) computation module (Phase C of iSHM) or Empirical CASD module (Phase C of mSHM). As the Phase C of iSHM is concerned, MLE computation method helps towards the MLE estimation of the applied CASDs given the coupling scheme channel attenuation differences of the Phase B [17], while the Phase C of mSHM computes the cumulative density function (CDF) given the coupling scheme channel attenuation differences of the Phase B [29].

The issue that this paper is dealing with is the underrepresentation of the aforementioned distribution BPL topology classes, as defined in this paper, through the insertion of virtual indicative OV and UN MV BPL topologies and their respective subclasses. In fact, the indicative distribution BPL topologies, which have been presented

in [17], [18], [29], also stand in this paper and define the respective main indicative distribution BPL topology subclasses as well as the titles of the respective distribution topology classes. As the operation of iSHM and mSHM is concerned, each indicative distribution BPL topology is characterized by a set of parameters regarding either iSHM (*i.e.,* MLEs) or mSHM (*i.e.,* Empirical CDF). Based on the set of parameters of an indicative distribution BPL topology, the respective main indicative distribution BPL topology subclass is filled with statistically equivalent BPL topologies, which are generated by a random number generator and are characterized by the same parameters with the representative topology of the examined main subclass for given power grid type, coupling scheme and CASD. In fact, by appropriately adjusting the parameters of iSHM and mSHM, new virtual indicative distribution BPL topologies can be proposed that further define their respective distribution BPL topology subclasses, which will further be enriched with statistically equivalent BPL topologies. In this paper, distribution BPL topology classes are defined as capacity areas (*i.e.,* capacity ranges) that comprise distribution BPL topology subclasses, whose average capacities lie in the middle of the distribution BPL topology class capacity ranges. Hence, distribution BPL topology classes will be filled with respective subclasses while the capacity ranges of distribution BPL topology classes are going to define valid combinations of parameters of iSHM and mSHM (CASD parameter mapping). On the basis of the CASD parameter mapping, virtual distribution BPL topology subclasses are identified while these subclasses are categorized into appropriate distribution BPL topology classes in terms of their average capacities (Subclass and Class Mapping). The numerical results of the full deployment of class mapping are presented: (i) for OV MV and UN MV BPL networks in [35]; and (ii) for OV high-voltage (HV) BPL networks in [36].

The rest of this paper is organized as follows: In Section II, the usual OV MV and UN MV MTL configurations with a set of indicative BPL topologies are presented. Section III summarizes the basics of the iSHM and mSHM. In Section IV, the definition procedure of the virtual indicative OV MV and UN MV BPL topologies and their respective virtual subclasses, briefly denoted as definition procedure, by adjusting CASD parameters of iSHM and mSHM is detailed. Section V concludes this paper.

2. OV MV and UN MV MTL Configurations and BPL Topologies

In this section, a small briefing regarding the applied OV MV and UN MV MTL configurations is given while the topological characteristics of the indicative OV MV and UN MV BPL topologies are reported. Note that these indicative distribution BPL topologies will act either as the reference topologies so that the capacity ranges of the distribution BPL topology classes are defined or representative topologies of the first respective distribution BPL topology subclasses of the corresponding BPL topology classes (main subclasses). Also, various distribution BPL topologies are presented that are going to be classified in the proposed distribution BPL topology classes and will further help the analysis.

2.1 OV MV and UN MV MTL Configurations
The OV MV and UN MV distribution lines that are used in the first two papers

are depicted in Figs. 1(a) and 1(b) of [17], respectively. As the OV MV distribution lines are concerned, these lines consists of three parallel non-insulated phase conductors ($n^{OVMV} = 3$) spaced by $\varDelta^{OVMV}$ and hang at typical heights h^{OVMV} above lossy ground. As the UN MV distribution lines are concerned, these lines are the three-phase sector-type PILC distribution-class cable (8/10kV, 3×95mm^2 Cu, PILC) surrounded by the shield and the armor conductor ($n^{UNMV} = 3$). The exact dimensions of the OV MV and UN MV MTL configurations are given in [30] as well as the ground properties, the applied grounding practices and the BPL signal propagation / transmission when a lossy ground is considered.

2.2 OV MV and UN MV BPL Topologies and Respective Topology Subclasses and Classes

With reference to Fig. 1, BPL networks are divided into cascaded BPL topologies. Each BPL topology is bounded by its transmitting and receiving end where BPL devices (*i.e.*, either injector or repeater or extractor) are installed. Depending on the power grid type environment of the BPL topology (*i.e.*, rural, suburban, urban or aggravated urban), different number of branches $k, \ k = 1, \cdots, N$, distribution cable lengths $L_k, \ k = 1, \cdots, N+1$ and branch lengths $L_{bk}, \ k = 1, \cdots, N$ are encountered across the BPL signal transmission path. To study distribution BPL topologies, hybrid model further divides the BPL topology into concatenated network modules [4], [23]-[27], [30].
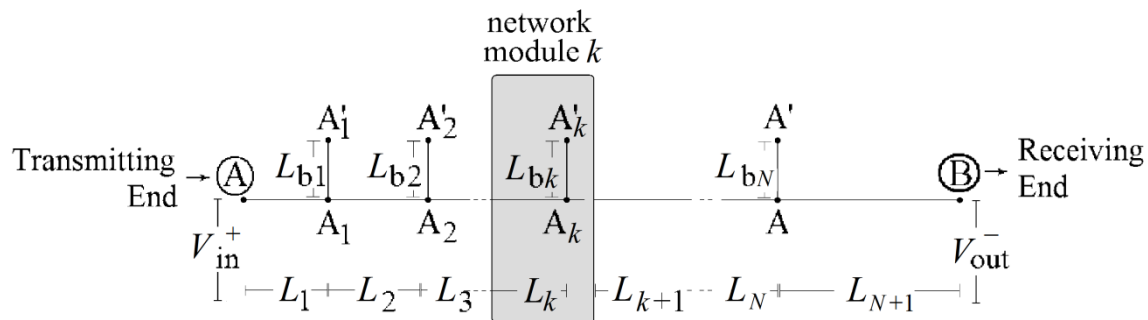

Fig. 1. Typical distribution BPL topology with N branches [17].

In accordance with [5], [17], [23]-[26], [30], five distribution BPL topology classes –*i.e.,* "Line-of-Sight" ("LOS"), rural, suburban, urban and aggravated urban– are required, so that a thorough analysis regarding the distribution BPL network performance is accomplished. Until now, an indicative distribution BPL topology has been adopted as the representative one for each distribution BPL topology class (say, urban case A, urban case B, suburban case, rural case and "LOS" case for distribution BPL typical urban, aggravated urban, suburban, rural and "LOS" topology class, respectively). In these papers, each indicative distribution BPL topology will act as the representative one for the main subclass of the respective distribution BPL topology class. In Tables 1 and 2, the indicative OV MV and UN MV BPL topologies of the main subclasses per each class, which are characterized by their unique topology number, are reported, respectively, as well as their corresponding topological characteristics. Also,

apart from the indicative OV MV and UN MV BPL topologies of the main subclasses per each class, two indicative OV MV and UN MV BPL topologies, which are also characterized by a unique topology number, are added per each OV MV and UN MV BPL topology class, respectively. Note that distribution "LOS" cases describe the Line-of-Sight BPL signal transmission path and for that reason, distribution "LOS" topology classes consist of only one topology; say, distribution "LOS" cases. In accordance with [5], [17], [23]-[26], [30], note that average long end-to-end connections of 1000 m and 200 m are assumed for the indicative OV MV and UN MV BPL topologies, respectively, as the typical case holds.

Table 1

Indicative OV MV BPL Topologies and Respective BPL Topology Classes [17], [5]

OV MV BPL Topology Class	BPL Topology Number (and BPL Topology Subclass Number) (l)	BPL Topology Name (and BPL Topology Subclass Name)	Number of Branches	Length of Distribution Lines	Length of Branching Lines
Typical OV MV BPL urban topology class	OV MV 1	OV MV Urban case A (main subclass)	3	L_1=500m, L_2=200m, L_3=100m, L_4=200m	L_{b1}=8m, L_{b2}=13m, L_{b3}=10m
Aggravated OV MV BPL urban topology class	OV MV 2	OV MV Urban case B (main subclass)	5	L_1=200m, L_2=50m, L_3=100m, L_4=200m, L_5=300m, L_6=150m	L_{b1}=12m, L_{b2}=5m, L_{b3}=28m, L_{b4}=41m, L_{b5}=17m
OV MV BPL suburban topology class	OV MV 3	OV MV Suburban case (main subclass)	2	L_1=500m, L_2=400m, L_3=100m	L_{b1}=50m, L_{b2}=10m
OV MV BPL rural topology class	OV MV 4	OV MV Rural case (main subclass)	1	L_1=600m, L_2=400m	L_{b1}=300m
OV MV BPL "LOS" topology class	OV MV 5	OV MV "LOS" case (main subclass)	0	L_1=1000m	-

Table 2
Indicative UN MV BPL Topologies and Respective BPL Topology Classes [17], [5]

| UN MV BPL Topology Class	BPL Topology Number (and BPL Topology Subclass Number) (l)	BPL Topology Name (and BPL Topology Subclass Name)	Number of Branches	Length of Distribution Lines	Length of Branching Lines
Typical UN MV BPL urban topology class	UN MV 1	UN MV Urban case A (main subclass)	3	L_1=70m, L_2=55m, L_3=45m, L_4=30m	L_{b1}=12m, L_{b2}=7m, L_{b3}=21m
Aggravated UN MV BPL urban topology class	UN MV 2	OV MV Urban case B (main subclass)	5	L_1=40m, L_2=10m, L_3=20m, L_4=40m, L_5=60m, L_6=30m	L_{b1}=22m, L_{b2}=12m, L_{b3}=8m, L_{b4}=2m, L_{b5}=17m
UN MV BPL suburban topology class	UN MV 3	UN MV Suburban case (main subclass)	2	L_1=50m, L_2=100m, L_3=50m	L_{b1}=60m, L_{b2}=30m
UN MV BPL rural topology class	UN MV 4	UN MV Rural case (main subclass)	1	L_1=50m, L_2=150m	L_{b1}=100m
UN MV BPL "LOS" topology class	UN MV 5	UN MV "LOS" case (main subclass)	0	L_1=200m	-

3. The Basics of iSHM and mSHM

In this Section, the flowcharts of iSHM and mSHM, which are given in terms of business process modeling notation (BPMN) diagrams, are demonstrated. On the basis of these BPMN diagrams, the Phases of iSHM and mSHM are presented while the required modifications for creating virtual distribution BPL topologies (*i.e.,* definition procedure of virtual distribution BPL topologies) are also given.

3.1 iSHM

The BPMN diagram of iSHM flowchart is presented in Fig. 2(a). In accordance with [17] and with respect to Fig. 1(a), iSHM consists of six phases; say, Phase A-F. Each phase is depicted as a grey container while their corresponding modules and produced files are shown in light blue color. iSHM receives as inputs the distribution power grid type, the indicative distribution BPL topology, the respective distribution MTL configuration, the applied coupling scheme and the capacity related parameters while it gives as output the capacity range of each distribution BPL topology subclass $\mathbf{CR}_l^{G,C,D} = \left[min\{\mathbf{c}_l^{G,C,D}\} \quad average\{\mathbf{c}_l^{G,C,D}\} \quad max\{\mathbf{c}_l^{G,C,D}\} \right]$ where $[\cdot]^G$ denotes the examined distribution power grid type (*i.e.,* OV MV or UN MV), $[\cdot]^C$ denotes the applied coupling scheme (see Sec.3.2 of [17]), $[\cdot]^D$ denotes the applied CASD (*i.e.,* Gaussian or Lognormal or Wald or Weibull or Gumbel distribution), $[\cdot]_l$ denotes the examined distribution BPL topology subclass number (see Tables 1 and 2) and $min\{\cdot\}$, $average\{\cdot\}$

and $max\{\cdot\}$ computes the minimum, the average and the maximum value of distribution BPL topology class capacity $\mathbf{C}_i^{G,C,D}$ that consists of all the capacities of its $P+1$ members of the examined distribution BPL topology subclass.
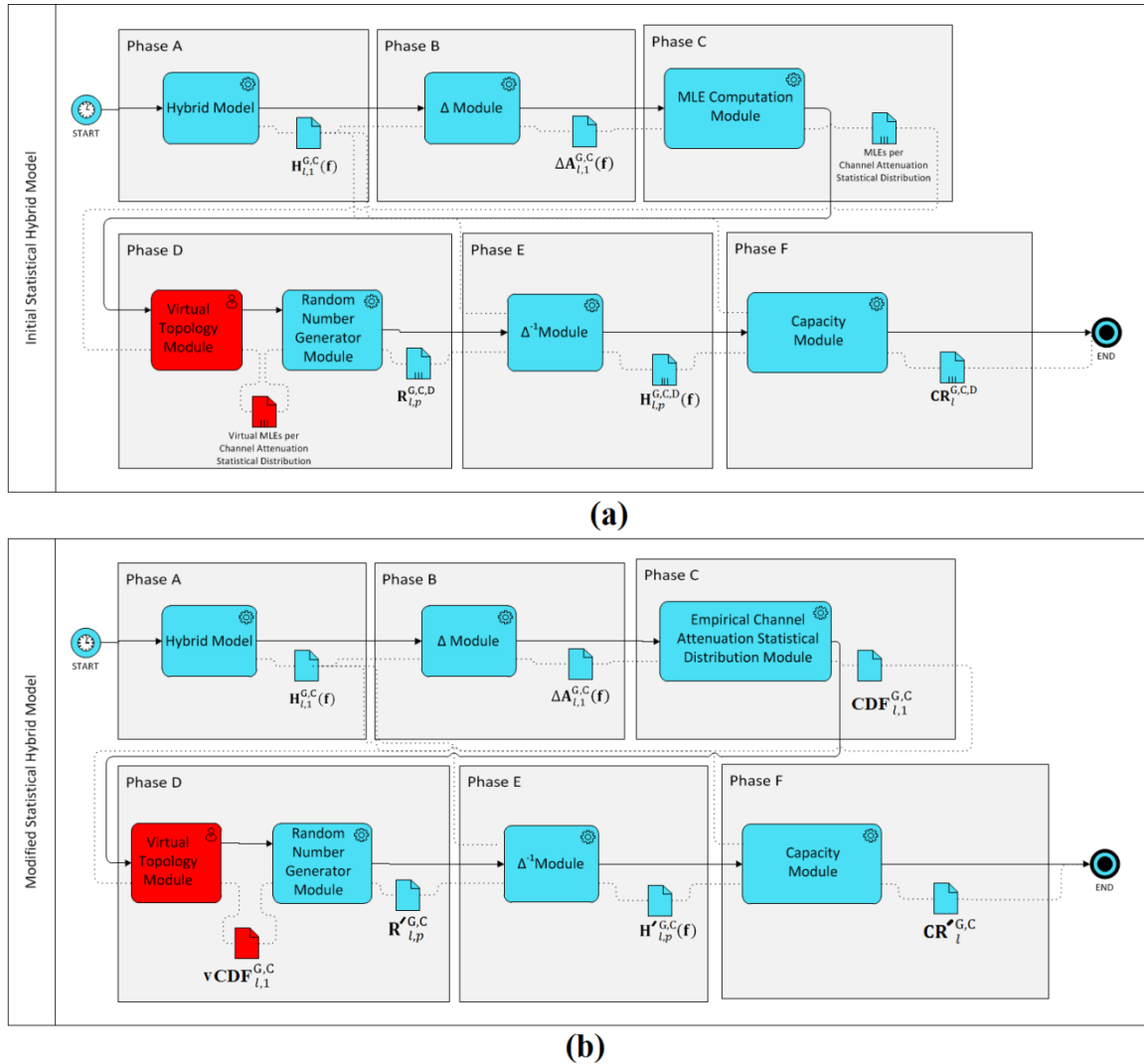
Fig. 2. Business Process Reengineering of the Statistical Hybrid Model. (a) BPMN diagram of the iSHM [17]. (b) BPMN diagram of the mSHM [29].

Although the Phases of iSHM and the input/output of iSHM are detailed in [17], the Phases that deserve further attention in this paper are Phases C and D since they are mainly affected by the definition procedure of virtual indicative OV MV and UN MV BPL topologies and their respective virtual subclasses. In fact, Phase C consists of the MLE computation module that receives as input the coupling scheme channel attenuation difference and gives as output the MLEs for each of the five CASDs for given indicative distribution BPL topology and coupling scheme where the coupling scheme channel attenuation difference of an indicative distribution BPL topology expresses the channel attenuation difference between the examined BPL topology and its respective "LOS"

case for given power grid type and coupling scheme. Then, the random number generator of Phase D receives as input the MLEs of each CASD and gives as output the random number $1 \times Q$ line vector $\mathbf{R}_{l,p}^{G,C,D}$ for given power grid type, coupling scheme and indicative distribution BPL topology where Q is the number of flat-fading subchannels in the examined 3-30MHz frequency range, $p, p=1,...,P+1$ is the member number in the BPL topology subclass and P is the member number of each subclass.

In Fig. 2(a), the additional BPMN elements, which will allow the application of the definition procedure of virtual indicative OV MV and UN MV BPL topologies and their respective virtual subclasses in iSHM, are shown in red color. More specifically, the required modifications of iSHM are gathered into the virtual topology module of Phase D. Then, the output of the virtual topology module (*i.e.*, virtual MLEs per channel attenuation statistical distribution) is delivered as the new input of the random number generator module. In fact, virtual topology module can operate by ignoring the MLEs per CASD so far defined by Phase A-C and introduce new pairs of MLEs (virtual MLEs) per CASD without the need for the applied indicative distribution BPL topology. Thus, the random number generator module is fed by virtual MLEs per CASD while it defines the corresponding P random number $1 \times Q$ line vectors $\mathbf{R}_{l,p}^{G,C,D}$ per virtual MLE pair set. In total, after the processing of the $P+1$ random number line vectors by the Phase E and F of the iSHM, a new virtual distribution BPL topology subclass rises with $P+1$ virtual topology members where the virtual indicative distribution BPL topology of the topology subclass is only characterized by its virtual MLEs proposed by the virtual topology module without any information concerning its topological characteristics.

In Sec.4.1, details concerning the operation of the virtual topology module of iSHM are given. More specifically, the definition procedure of virtual MLEs per CASD is presented as well as the restrictions that should be imposed so that valid virtual distribution BPL topologies can be defined in iSHM.

3.2 mSHM

The introduction of mSHM focuses on the application of only one CASD, say, the Empirical CASD, thus bypassing the time-consuming identification of the best CASD among the five CASDs of iSHM that anyway takes into consideration each time the current operation settings. Here it should be noted that the Empirical CASD is the distribution function associated with the Empirical measure of coupling scheme channel attenuation differences.

The BPMN diagram of mSHM flowchart is presented in Fig. 2(b). In accordance with [29] and with respect to Figs. 2(a) and 2(b), mSHM consists of six phases; say, Phase A-F, similarly to iSHM. Each phase is depicted as a grey container while their corresponding modules and produced files are shown in light blue color. Actually, Phases A, B, E and F remain identical between the iSHM and mSHM. Conversely, the cause of differences in the Phases C and D between iSHM and mSHM is the adoption of the Empirical CASD by mSHM. In fact, the adoption of Empirical CASD, which is only used by mSHM, has as a result the substitution of all the five applied CASDs of iSHM (*i.e.*, Gaussian or Lognormal or Wald or Weibull or Gumbel distribution). In accordance with [29], the adoption of Empirical CASD achieves comparable performances to the ones of the five applied CASDs of iSHM and, at the same time, this adoption bypasses the time loss required to identify the best CASD of iSHM by taking into consideration

each time the current operation settings. As the Phase differences between iSHM and mSHM are concerned, instead of the MLE computation module of iSHM in Phase C, the Empirical channel attenuation statistical distribution module is here added for mSHM that receives as input the coupling scheme channel attenuation difference while it gives as output the empirical CDF of the coupling scheme channel attenuation difference $\mathbf{CDF}_{l,1}^{G,C}$ for given distribution BPL topology and coupling scheme. In Phase D of mSHM, the random number generator receives as input the Empirical CDF of the examined coupling scheme channel attenuation difference instead of MLEs in iSHM. With reference to [37], [38], random number generator module performs an inverse interpolation to achieve CDF projection of the random values thus giving as output the random number $1 \times Q$ line vector $\mathbf{R}_{l,p}^{\prime G,C}$ for given coupling scheme and indicative distribution BPL topology.

Similarly to iSHM, the additional BPMN elements, which will allow the application of the definition procedure of virtual indicative OV MV and UN MV BPL topologies and their respective virtual subclasses in mSHM, are shown in red color in Fig. 2(b). Again, the required modifications of mSHM are gathered into the virtual topology module of Phase D. In contrast with iSHM, the output of the virtual topology module that is a virtual CDF is delivered as the new input of the random number generator module. To operate, virtual topology module needs CDF so far defined by Phase A-C and can introduce new CDFs (virtual CDFs) by vertically and horizontally shifting CDF of the applied indicative distribution BPL topology. Thus, the random number generator module is fed by virtual CDFs while it defines the corresponding P random number $1 \times Q$ line vectors $\mathbf{R}_{l,p}^{\prime G,C}$. In total, the new virtual distribution BPL topology subclass of mSHM with $P+1$ virtual topology members is defined where the virtual indicative distribution BPL topology of the topology subclass is only characterized by its virtual Empirical CDF proposed by the virtual topology module without any information concerning its topological characteristics.

In Sec.4.2, details concerning the operation of the virtual topology module of mSHM are given. More specifically, the definition procedure of a virtual CDF per indicative distribution BPL topology is presented in mathematical terms as well as the restrictions that should be imposed to the horizontal and vertical shifts of the virtual CDF so that valid virtual distribution BPL topologies can be defined in mSHM.

4. CASD Parameters Adjustment for Defining Virtual Distribution BPL Topologies and Respective Subclasses

In this Section, the definition procedure of the virtual indicative OV MV and UN MV BPL topologies and their respective virtual subclasses by adjusting CASD parameters of iSHM and mSHM is detailed while the required restrictions concerning the proper definition are presented.
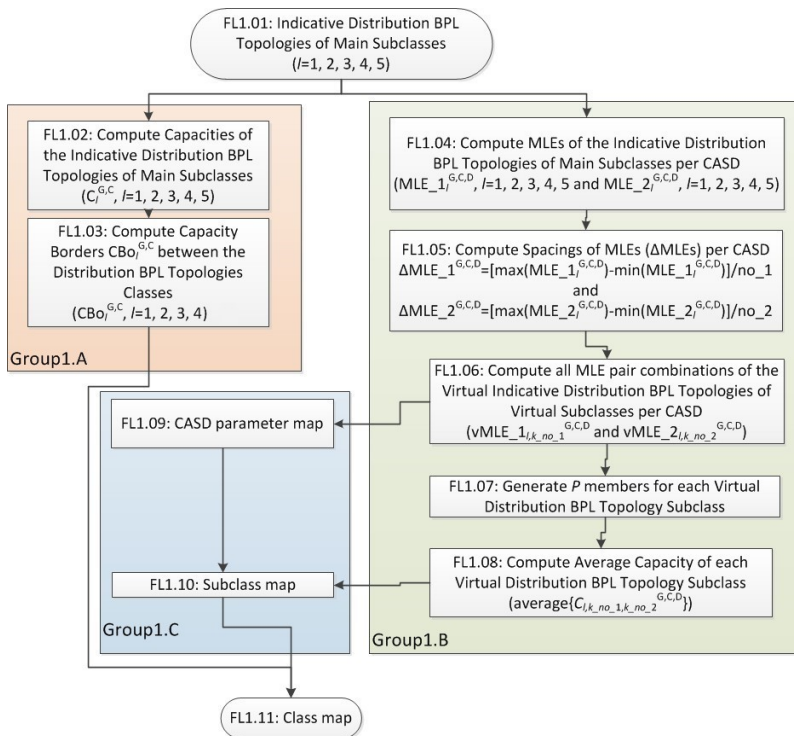
(a)
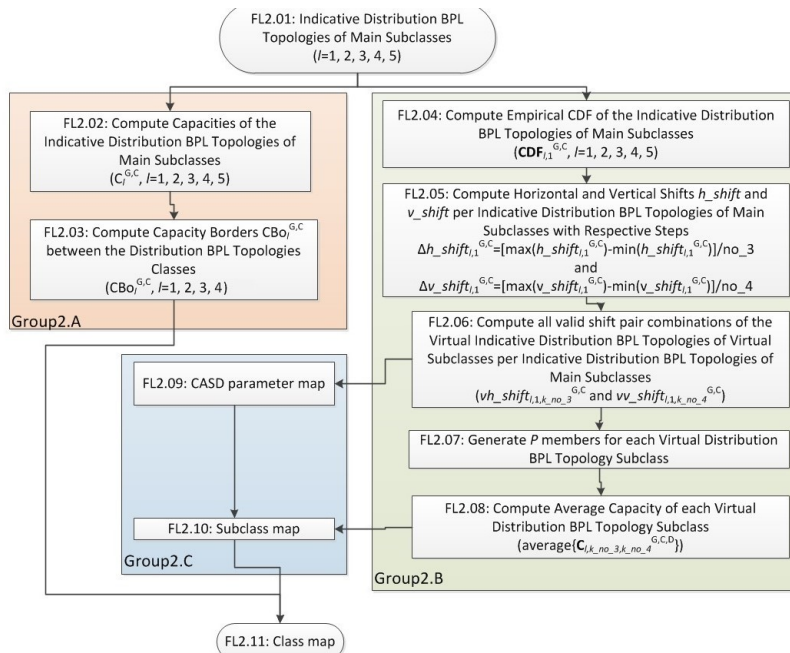
(b)

Fig. 3. Flowcharts of the CASD parameter adjustment for defining virtual distribution BPL topologies and subclasses of the Statistical Hybrid Model.
(a) Definition procedure flowchart for the iSHM. (b) Definition procedure flowchart for the mSHM.

4.1 Definition Procedure of iSHM

Actually, in this subsection, the operation of the virtual topology module of Phase D of Fig. 2(a) is studied as well as its output, say virtual MLEs per CASD. In fact, the internal operation of the virtual topology module cannot be seen without the flow of its output until the end and for that reason all this procedure is demonstrated through the flowchart of Fig. 3(a).

In accordance with Fig. 3(a), there are eleven steps so that the class map, which is the result of the definition procedure, can be plotted where class map is a two-dimensional contour plot that depicts the average capacity of each possible virtual distribution BPL topology subclass classified in specific classes. Note that indicative distribution BPL topologies of main subclasses of Tables 1 and 2 are explicitly demonstrated in the class map while these BPL topologies become crucial for defining the borders between the adjacent distribution BPL topology classes as presented in the following analysis. With reference to Fig. 3(a), after the definition of the indicative distribution BPL topologies of main subclasses of Tables 1 and 2 (step FL1.01), the result of class mapping is accomplished through three groups of steps, namely:

1. *Group1.A*: This group consists of two steps (FL1.02 and FL1.03). First, the capacities of the indicative distribution BPL topologies of main subclasses $C_l^{G,C}, l = 1,2,3,4,5$ are computed in the step FL1.02. Second, given the capacities of the indicative distribution BPL topologies of main subclasses from FL1.02, which anyway act as the representative BPL topologies of the respective distribution BPL topology classes, the capacity borders between the adjacent distribution BPL topology classes $CBo_l^{G,C}, l = 1,2,3,4$ are determined by

$$\mathbf{CBo}^{G,C} = \left[CBo_l^{G,C}\right], l = 1,2,3,4 = \left[\frac{C_{1,1}^{G,C}+C_{2,1}^{G,C}}{2} \quad \frac{C_{1,1}^{G,C}+C_{3,1}^{G,C}}{2} \quad \frac{C_{3,1}^{G,C}+C_{4,1}^{G,C}}{2} \quad C_5^{G,C}\right] \quad (1)$$

From eq. (1), it is evident that $CBo_4^{G,C}$, which is equal to the capacity of the distribution BPL "LOS" topology case $C_5^{G,C}$, describes the capacity upper limit that can be achieved for given power grid type and coupling scheme. As the other distribution BPL topology class capacity borders are considered, these are treated as the mean capacity value of the neighboring indicative distribution BPL topologies of the main subclasses of Tables 1 and 2. Note that $CBo_l^{G,C}, l = 1,2,3,4$ describe the borders: (i) between the aggravated distribution BPL urban topology class and typical distribution BPL urban topology class; (ii) between the typical distribution BPL urban topology class and the distribution BPL suburban topology class; (iii) between the typical distribution BPL suburban topology class and the distribution BPL rural topology class; (iv) between the typical distribution BPL rural topology class and the distribution BPL "LOS" topology class; and (v) the upper capacity bound that is equal to the capacity of the distribution BPL "LOS" case, respectively. In total, the capacities of the indicative distribution BPL topologies of main subclasses and the capacity borders between the adjacent distribution BPL topology classes remain crucial elements during the class mapping since they define the placement of the capacities of the virtual distribution BPL topology subclasses.

2. *Group1.B*: This group consists of five steps (FL1.04-FL1.08). At step FL1.04, the MLE estimation of the applied CASD given the coupling scheme channel

attenuation differences of the examined distribution BPL topology is accomplished at Phase B of iSHM, as described in Fig. 2(a). Actually, according to the step FL1.04, the MLE computation module provides a MLE pair given the indicative distribution BPL topologies of main subclasses of Tables 1 and 2 per CASD. Literally, each MLE pair of the indicative distribution BPL topologies of the main subclasses per CASD consists of $MLE\_1_l^{G,C,D}, l = 1, 2, 3, 4, 5$ and $MLE\_2_l^{G,C,D}, l = 1, 2, 3, 4, 5$. At step FL1.05, the accuracy of the class mapping can be adjusted by the length of horizontal and vertical spacings, say

$$\Delta MLE\_1_l^{G,C,D} = \frac{max\{MLE\_1_l^{G,C,D}\} - min\{MLE\_1_l^{G,C,D}\}}{no\_1}, l = 1, 2, 3, 4, 5 \quad (2)$$

$$\Delta MLE\_2_l^{G,C,D} = \frac{max\{MLE\_2_l^{G,C,D}\} - min\{MLE\_2_l^{G,C,D}\}}{no\_2}, l = 1, 2, 3, 4, 5 \quad (3)$$

, respectively, where no_1 and no_2 are the number of spacings for the horizontal and vertical axis, respectively. At step FL1.06, all $(no\_1 + 1) \times (no\_2 + 1)$ MLE pair combinations of the virtual indicative distribution BPL topologies of virtual classes per CASD $[vMLE\_1_{l,k\_no\_1}^{G,C,D} \quad vMLE\_2_{l,k\_no\_1}^{G,C,D}], k\_no\_1 = 0,1, \cdots, no\_1, k\_no\_2 = 0,1, \cdots, no\_2$

, which are anyway computed by taking into account the horizontal and vertical spacings of eqs. (2) and (3), respectively, are computed, namely:

$$vMLE\_1_{l,k\_no\_1}^{G,C,D} = min\{MLE\_1_l^{G,C,D}\} + k\_no\_1 \cdot \Delta MLE\_1_l^{G,C,D}, l = 1, 2, 3, 4, 5,$$
$$k\_no\_1 = 0,1, \cdots, no\_1 \quad (4)$$

$$vMLE\_2_{l,k\_no\_2}^{G,C,D} = min\{MLE\_2_l^{G,C,D}\} + k\_no\_2 \cdot \Delta MLE\_2_l^{G,C,D}, l = 1, 2, 3, 4, 5,$$
$$k\_no\_2 = 0,1, \cdots, no\_2 \quad (5)$$

Anyway, MLE pair combinations of the virtual indicative distribution BPL topologies of virtual subclasses per CASD are considered as the output of the virtual topology module of Phase D of Fig. 2(a) and as the essential modification of iSHM towards the enrichment of the distribution BPL topology subclasses. In fact, at step FL1.07, the random number generator of Phase D of Fig.2(a) exploits the MLE pair combinations of the virtual indicative distribution BPL topologies of virtual classes per CASD and it generates P members for each distribution BPL topology subclass. Finally, step FL1.08 synopsizes the operation of Phases E and F of iSHM as described in Fig. 2(a) while the output of step FL1.08 is the average capacity value average$\{ C_{l,k\_no\_1,k\_no\_2}^{G,C,D} \}$, $k\_no\_1 = 0,1, \cdots, no\_1$, $k\_no\_2 = 0,1, \cdots, no\_2$ of each distribution BPL topology subclass. The output of steps FL1.06 and FL1.08 seed the Group1.C that is responsible for the mapping of the results.

3. *Group1.C*. This group consists of two steps (FL1.09 and FL1.10) and is the responsible one for the class mapping. First, step FL1.09 receives as input the output of the step FL1.06, say, all $(no\_1 + 1) \times (no\_2 + 1)$ MLE pair combinations of the virtual indicative distribution BPL topologies of virtual classes per CASD $[vMLE\_1_{l,k\_no\_1}^{G,C,D} \quad vMLE\_2_{l,k\_no\_1}^{G,C,D}], k\_no\_1 = 0,1, \cdots, no\_1, k\_no\_2 = 0,1, \cdots, no\_2$
. Hence, the minimum and maximum values of horizontal and vertical axes of the

2D contour plot of the class map are well defined per CASD as well as all the possible combinations of the horizontal and vertical values. This procedure is denoted as CASD parameter mapping. Second, FL1.10 receives: (i) the CASD parameters from FL1.09; and (ii) the average capacity values $\text{average}\{C_{l,k\_no\_1,k\_no\_2}^{G,C,D}\}$, $k\_no\_1 = 0, 1, \cdots, no\_1$, $k\_no\_2 = 0, 1, \cdots, no\_2$ of each distribution BPL topology subclass that correspond to all possible combinations of horizontal values k_no_1 and vertical values k_no_2. Actually, the existing CASD parameter map of FL1.09 is enriched by the average capacities of all distribution BPL topology subclasses and the subclass map is treated as the output of FL1.10 and, thus, Group1.C.

The last step of the definition procedure of the virtual indicative OV MV and UN MV BPL topologies and their respective virtual subclasses is step FL1.11. By synthesizing its inputs into a 2D contour plot, step FL1.11 receives the CASD parameter map from Group1.C and the capacities of the indicative distribution BPL topologies of main subclasses accompanied with the capacity borders between the adjacent distribution BPL topology classes from Group1.A and gives as output the class map that is the result of the definition procedure of the virtual indicative OV MV and UN MV BPL topologies and their respective virtual subclasses of iSHM.

4.2 Definition Procedure of mSHM

Similarly to iSHM, in this subsection, the operation of the virtual topology module of Phase D of Fig. 2(b) is studied as well as its output. Conversely to virtual MLEs per CASD of iSHM, the output of the virtual tropology module of mSHM is the virtual Empirical CDF $\mathbf{vCDF}_{l,1}^{G,C}$, $l = 1, 2, 3, 4, 5$ of the examined coupling scheme channel attenuation difference. Similarly to Sec.4.1, the flow of the virtual topology module of Phase D until the end is demonstrated through the flowchart of Fig. 3(b).

In accordance with Fig. 3(b), class mapping consists of eleven steps (FL2.01-FL2.11) that are further classified into three groups (Group2.A-Group2.C). Similarly to the definition procedure of iSHM of Fig. 3(a), with reference to Fig. 3(b), after the definition of the indicative distribution BPL topologies of main subclasses of Tables 1 and 2 (step FL2.01), the result of class mapping is accomplished through three groups of steps, namely:

1. *Group2.A*: This group consists of two steps (FL2.02 and FL2.03). Both FL2.02 and FL2.03 are the same with FL1.02 and FL1.03, respectively. In general, the input of the definition procedure of mSHM, which is the output of the step FL2.01, remains the same one with the definition procedure of iSHM and the output of the definition procedure of mSHM, which is the capacity borders between the adjacent distribution BPL topology classes $CBo_l^{G,C}$, $l = 1, 2, 3, 4, 5$ as given in eq.(1), again remains the same one with the definition procedure of iSHM.

2. *Group2.B*: This group consists of five steps (FL2.04-FL2.08). At step FL2.04, the Empirical CDFs $\mathbf{CDF}_{l,1}^{G,C}$, $l = 1, 2, 3, 4, 5$ of the indicative distribution BPL topologies of main subclasses are delivered by the Empirical Channel Attenuation Statistical Distribution module of Phase C of mSHM. Similarly to the role of CASD selection of iSHM, the selection of the reference distribution BPL

topology among the available indicative distribution BPL topologies of the main subclasses will define either the calculations of FL2.05-FL2.08 or the final class map. At step FL2.05, the Empirical CDF of the virtual distribution BPL topologies of subclasses can be adjusted by the spacing of horizontal shift $h\_shift_{l,1}^{G,C}$ and vertical shift $v\_shift_{l,1}^{G,C}$ of the Empirical CDFs; the horizontal shift $h\_shift_{l,1}^{G,C}$ ranges from $min\{h\_shift_{l,1}^{G,C}\}$ to $max\{h\_shift_{l,1}^{G,C}\}$ with step

$$\Delta h\_shift_{l,1}^{G,C} = \frac{max\{h\_shift_{l,1}^{G,C}\} - min\{h\_shift_{l,1}^{G,C}\}}{no\_3}, l = 1,2,3,4,5 \qquad (6)$$

while the vertical shift $v\_shift_{l,1}^{G,C}$ ranges from $min\{v\_shift_{l,1}^{G,C}\}$ to $max\{v\_shift_{l,1}^{G,C}\}$ with step

$$\Delta v\_shift_{l,1}^{G,C} = \frac{max\{v\_shift_{l,1}^{G,C}\} - min\{v\_shift_{l,1}^{G,C}\}}{no\_4}, l = 1,2,3,4,5 \qquad (7)$$

where no_3 and no_4 are the number of spacings for the horizontal and vertical axis, respectively. Given the horizontal and vertical shift spacings of eqs. (6) and (7), the possible horizontal and vertical spacings can be computed by:

$$vh\_shift_{l,1,k\_no\_3}^{G,C} = min\{h\_shift_{l,1}^{G,C}\} + k\_no\_3 \cdot \Delta h\_shift_{l,1}^{G,C}, l = 1,2,3,4,5,$$
$$k\_no\_3 = 0,1,\cdots,no\_3 \qquad (8)$$

$$vv\_shift_{l,1,k\_no\_4}^{G,C} = min\{v\_shift_{l,1}^{G,C}\} + k\_no\_4 \cdot \Delta v\_shift_{l,1}^{G,C}, l = 1,2,3,4,5,$$
$$k\_no\_4 = 0,1,\cdots,no\_4 \qquad (9)$$

, respectively. In order to explain the operation of the horizontal and vertical shifts during the definition of the Empirical CDF of a virtual distribution BPL topology, there is first the need for understanding the definition of the Empirical CDF of the reference indicative distribution BPL topology by the Empirical channel attenuation statistical distribution module of Phase C, as presented in Fig. 2(b). In fact, with reference to Phase B of Fig. 2(b), Phase C receives as input the $1 \times Q$ line vector coupling scheme channel attenuation difference between the reference indicative distribution BPL topology l and its respective "LOS" case, say

$$\Delta \mathbf{A}_{l,1}^{G,C}(\mathbf{f}) = -[\mathbf{H}_{l,1}^{G,C}(\mathbf{f}) - \mathbf{H}_{5,1}^{G,C}(\mathbf{f})] \qquad (10)$$

In fact, the Empirical CDF $\mathbf{CDF}_{l,1}^{G,C}$ is an increasing function of the coupling scheme channel attenuation difference between the reference indicative distribution BPL topology l and its respective "LOS" case $\Delta \mathbf{A}_{l,1}^{G,C}(\mathbf{f})$ sorted in ascending order, say $\mathbf{CDF}_{l,1}^{G,C}\left(\left\{\Delta \mathbf{A}_{l,1}^{G,C}(\mathbf{f})\right\}_{asc}\right)$ where $\{\cdot\}_{asc,q}$ is an operator that sorts a line vector in ascending order and returns the element at row q. Note that the number of elements of line vector $\left\{\Delta \mathbf{A}_{l,1}^{G,C}(\mathbf{f})\right\}_{asc}$ is equal to Q reduced by the number of duplicate values dv_1. Hence, the Empirical CDF $\mathbf{CDF}_{l,1}^{G,C}$ consists of the elements $CDF_{l,1,q}^{G,C}\left(\left\{\Delta A_{l,1}^{G,C}(\mathbf{f})\right\}_{asc,q}\right)$, $q = 1,\cdots,Q - dv_1$. At step FL2.06, all the shift pair combinations of the virtual indicative distribution BPL topologies of virtual subclasses per indicative distribution BPL topology of main subclass $\left[vh\_shift_{l,1,k\_no\_3}^{G,C} \quad vv\_shift_{l,1,k\_no\_4}^{G,C}\right], k\_no\_3 = 0,1,\cdots,no\_3, k\_no\_4 = 0,1,\cdots,no\_4$

are first computed as well as the virtual Empirical CDF $\mathbf{vCDF}_{l,1}^{G,C}$ per each shift pair combination. In general, virtual Empirical CDF is a

$(no\_3 + 1) \times (no\_4 + 1) \times (Q - dv_1 - dv_2)$ array while Empirical CDF can be treated as a $1 \times (Q - dv_1 - dv_2)$ line vector for given horizontal and vertical shift pair. Empirical CDF consists of $vCDF_{l,1,q}^{G,C}$, $q = 1, \cdots, Q - dv_1 - dv_2$, is related with the Empirical CDF of the reference indicative distribution BPL topology and depends on the horizontal shift $vh\_shift_{l,1,k\_no\_3}^{G,C}$ and vertical shift $vv\_shift_{l,1,k\_no\_4}^{G,C}$, namely:

$$vCDF_{l,1,q}^{G,C}\left(vh\_shift_{l,1,k\_no\_3}^{G,C}, vv\_shift_{l,1,k\_no\_4}^{G,C}, max\left\{1 \times 10^{-11}, \left\{\Delta A_{l,1}^{G,C}(f)\right\}_{asc,q}\right.\right.$$
$$\left.\left. + vh\_shift_{l,1,k\_no\_3}^{G,C}\right\}\right)$$
$$= min\left\{CDF_{l,1,q}^{G,C}\left(\left\{\Delta A_{l,1}^{G,C}(f)\right\}_{asc,q}\right) + vv\_shift_{l,1,k\_no\_4}^{G,C}, 1\right\},$$
$$q = 1, \cdots, Q - dv_1 - dv_2, k\_no\_3 = 0,1, \cdots, no\_3, k\_no\_4 = 0,1, \cdots, no\_4 \quad (11)$$

where dv_2 is the number of duplicate values of $\mathbf{vCDF}_{l,1}^{G,C}(vh\_shift_{l,1,k\_no\_3}^{G,C}, vv\_shift_{l,1,k\_no\_4}^{G,C})$.

Note that eq.(11) synopsizes all the necessary checks from FL2.06 so that valid shift pair combinations can be defined, namely:

- *Non-negative coupling scheme channel attenuation differences for the Virtual Empirical CDFs*. As already been mentioned in [17], [18], only values greater or equal than zero are expected for the coupling scheme channel attenuation differences while in the scarce cases of negative coupling scheme channel attenuation differences and in "LOS" cases, the coupling scheme channel attenuation differences are assumed to be equal to an arbitrarily low value, say 1×10^{-11}. Instead of zero, the value 1×10^{-11} has been assumed in [18] so that MLEs of Lognormal, Wald and Weibull channel attenuation distributions, which comprise natural logarithms and denominators, can be calculated and for that reason this assumption is also made in this paper through $max\left\{1 \times 10^{-11}, \left\{\Delta A_{l,1}^{G,C}(f)\right\}_{asc,q} + vh\_shift_{l,1,k\_no\_3}^{G,C}\right\}$ of eq.(11). Note that this assumption is not assumed during the computation of MLEs of indicative distribution "LOS" cases that was anyway out of the scope of [17], [18] but is of interest in these papers.

- *The maximum value of a CDF is equal to 1*. By definition, the maximum value of a CDF is equal to 1 and, for that reason, the virtual empirical CDF is upper bounded by $min\left\{CDF_{l,1,q}^{G,C}\left(\left\{\Delta A_{l,1}^{G,C}(f)\right\}_{asc,q}\right) + vv\_shift_{l,1,k\_no\_4}^{G,C}, 1\right\}$ of eq.(11) for given horizontal and vertical shift.

At step FL2.07, the random number generator of Phase D of Fig.2(b) exploits the Empirical CDF of the virtual indicative distribution BPL topologies of virtual main subclasses per horizontal and vertical shift set and it generates P members for each distribution BPL topology subclass. Finally, step FL2.08 synopsizes the operation of Phases E and F of mSHM as described in Fig. 2(b) while the output of step FL2.08 is the average capacity value average$\{C_{l,k\_no\_3,k\_no\_4}^{G,C,D}\}$, $k\_no\_3 = 0,1, \cdots, no\_3$, $k\_no\_4 = 0,1, \cdots, no\_4$ of each distribution BPL topology subclass. Similarly to the definition procedure of iSHM, the output of

steps FL2.06 and FL2.08 seed the Group2.C that is responsible for the mapping of the results.

3. *Group2.C.* Similarly to Group1.C of iSHM, this group consists of two steps (FL2.09 and FL2.10) and is the responsible group for the class mapping. First, step FL2.09 receives as input the output of the step FL2.06, say, all $(no\_3 + 1) \times (no\_4 + 1)$ shift pair combinations of the virtual indicative distribution BPL topologies of virtual classes per representative indicative distribution BPL topology of the main subclasses $\left[vh\_shift_{l,1,k\_no\_3}^{G,C} \quad vv\_shift_{l,1,k\_no\_4}^{G,C}\right], k\_no\_3 = 0,1,\cdots,no\_3, k\_no\_4 = 0,1,\cdots,no\_4$
. Hence, the minimum and maximum values of horizontal and vertical axes of the 2D contour plot of the class map are well defined per representative indicative distribution BPL topology of the main subclasses as well as all the possible combinations of the horizontal and vertical values. This procedure is denoted as CASD parameter mapping. Second, FL2.10 receives: (i) the CASD parameters from FL2.09; and (ii) the average capacity values $\text{average}\{C_{l,k\_no\_3,k\_no\_4}^{G,C,D}\}, k\_no\_3 = 0,1,\cdots,no\_1, k\_no\_4 = 0,1,\cdots,no\_2$ of each distribution BPL topology subclass that correspond to all possible combinations of horizontal values k_no_3 and vertical values k_no_4 . Actually, average capacities of all distribution BPL topology subclasses enrich the existing CASD parameter map of FL2.09. The existing contour plot is the subclass map that is delivered by the step FL2.11.

The last step of the definition procedure of the virtual indicative OV MV and UN MV BPL topologies and their respective virtual subclasses is step FL2.11. The output of the step FL2.11 that coincides with the output of the definition procedure of mSHM is the synthesis of inputs of the current step into a 2D contour plot. Similarly to iSHM, step FL2.11 receives the CASD parameter map from Group2.C and the capacity borders between the adjacent distribution BPL topology classes from Group2.A and gives as output the class map that is the result of the definition procedure of the virtual indicative OV MV and UN MV BPL topologies and their respective virtual subclasses of mSHM.

Synopsizing this Section, the definition procedure of the virtual indicative distribution BPL topologies and their respective virtual subclasses by adopting iSHM and mSHM allows the class enrichment with distribution BPL topologies that are statistically tested without the need for searching topological characteristic combinations that may fit any performance requirements. By consulting the class map and selecting appropriate CASD parameters, coupling channel attenuation and capacity data can be assumed for any class and further being processed. Finally, it is obvious that power grid types and the two different versions of SHM have different impact on class maps and to investigate the result behavior of the definition procedure, numerical results are presented in the companion paper of [35] for OV MV and UN MV BPL topologies. In [36], iSHM and mSHM are first applied to OV HV BPL networks while the results of the definition procedure and the class map are first demonstrated.

5. Conclusions

In this paper, the definition procedure of virtual indicative OV MV and UN MV BPL topologies and their respective virtual subclasses has been analyzed through the prism of iSHM and mSHM. In fact, on the basis of the theoretical framework and the BPMN diagrams of iSHM and mSHM, the respective definition procedure flowcharts have been proposed as well as the required theoretical framework. As the theory of the definition procedure is concerned, it has been shown that the definition procedures of iSHM and mSHM consist of three groups and eleven steps each where the statistical processing and the graphical representation of indicative distribution BPL topologies are accomplished. By exploiting the knowledge of the deterministic hybrid model, iSHM and mSHM, CASD parameter map, subclass map and class map have been proposed. Class map, which is a 2D contour plot and the output of the definition procedure, illustrates the borders between the neighboring distribution BPL topology classes and correspond each CASD parameter pair to its distribution BPL topology subclass average capacity for given power grid type, coupling scheme, IPSD limits and noise levels. The numerical results of the definition procedure are presented for distribution and transmission BPL networks in [35] and [36], respectively.

CONFLICTS OF INTEREST

The author declares that there is no conflict of interests regarding the publication of this paper.

References

[1]   A. G. Lazaropoulos, "Factors Influencing Broadband Transmission Characteristics of Underground Low-Voltage Distribution Networks," *IET Commun.*, vol. 6, no. 17, pp. 2886-2893, Nov. 2012.

[2]   F. Aalamifar and L. Lampe, "Optimized WiMAX profile configuration for smart grid communications," *IEEE Transactions on Smart Grid*, vol. 8, no. 6, pp. 2723-2732, 2017.

[3]   A. G. Lazaropoulos, "Deployment Concepts for Overhead High Voltage Broadband over Power Lines Connections with Two-Hop Repeater System: Capacity Countermeasures against Aggravated Topologies and High Noise Environments," *Progress in Electromagnetics Research B*, vol. 44, pp. 283-307, 2012. [Online]. Available: http://www.jpier.org/PIERB/pierb44/13.12081104.pdf

[4]   A. G. Lazaropoulos, "Towards Broadband over Power Lines Systems Integration: Transmission Characteristics of Underground Low-Voltage Distribution Power Lines," *Progress in Electromagnetics Research B*, vol. 39, pp. 89-114, 2012. [Online]. Available: http://www.jpier.org/PIERB/pierb39/05.12012409.pdf

[5]   A. G. Lazaropoulos, "Broadband Performance Metrics and Regression Approximations of the New Coupling Schemes for Distribution Broadband over Power Lines (BPL) Networks," *Trends in Renewable Energy*, vol. 4, no. 1, pp.

43-73,   Jan.   2018.   [Online].   Available:
http://futureenergysp.com/index.php/tre/article/view/59/pdf

[6]   A. G. Lazaropoulos, "Wireless Sensor Network Design for Transmission Line Monitoring, Metering and Controlling Introducing Broadband over PowerLines-enhanced Network Model (BPLeNM)," *ISRN Power Engineering*, vol. 2014, Article ID 894628, 22 pages, 2014. doi:10.1155/2014/894628. [Online]. Available:
http://www.hindawi.com/journals/isrn.power.engineering/2014/894628/

[7]   A. G. Lazaropoulos, "Improvement of Power Systems Stability by Applying Topology Identification Methodology (TIM) and Fault and Instability Identification Methodology (FIIM)–Study of the Overhead Medium-Voltage Broadband over Power Lines (OV MV BPL) Networks Case," *Trends in Renewable Energy*, vol. 3, no. 2, pp. 102-128, Apr. 2017. [Online]. Available:
http://futureenergysp.com/index.php/tre/article/view/34

[8]   A. G. Lazaropoulos, "Main Line Fault Localization Methodology in Smart Grid–Part 1: Extended TM2 Method for the Overhead Medium-Voltage Broadband over Power Lines Networks Case," *Trends in Renewable Energy*, vol. 3, no. 3, pp. 2-25,   Dec.   2017.   [Online].   Available:
http://futureenergysp.com/index.php/tre/article/view/36

[9]   A. G. Lazaropoulos, "Main Line Fault Localization Methodology in Smart Grid–Part 2: Extended TM2 Method, Measurement Differences and L1 Piecewise Monotonic Data Approximation for the Overhead Medium-Voltage Broadband over Power Lines Networks Case," *Trends in Renewable Energy*, vol. 3, no. 3, pp. 26-61,   Dec.   2017.   [Online].   Available:
http://futureenergysp.com/index.php/tre/article/view/37

[10]   A. G. Lazaropoulos, "Main Line Fault Localization Methodology in Smart Grid–Part 3: Main Line Fault Localization Methodology (MLFLM)," *Trends in Renewable Energy*, vol. 3, no. 3, pp. 62-81, Dec. 2017. [Online]. Available:
http://futureenergysp.com/index.php/tre/article/view/38

[11]   A. G. Lazaropoulos, "Main Line Fault Localization Methodology (MLFLM) in Smart Grid–The Underground Medium- and Low-Voltage Broadband over Power Lines Networks Case," *Trends in Renewable Energy*, vol. 4, no. 1, pp. 15-42, Dec.   2017.   [Online].   Available:
http://futureenergysp.com/index.php/tre/article/view/45

[12]   A. G. Lazaropoulos, "Smart Energy and Spectral Efficiency (SE) of Distribution Broadband over Power Lines (BPL) Networks – Part 1: The Impact of Measurement Differences on SE Metrics," *Trends in Renewable Energy*, vol. 4, no.   2,   pp.   125-184,   Aug.   2018.   [Online].   Available:
http://futureenergysp.com/index.php/tre/article/view/76/pdf

[13]   A. G. Lazaropoulos, "Smart Energy and Spectral Efficiency (SE) of Distribution Broadband over Power Lines (BPL) Networks – Part 2: L1PMA, L2WPMA and L2CXCV for SE against Measurement Differences in Overhead Medium-Voltage BPL Networks," *Trends in Renewable Energy*, vol. 4, no. 2, pp. 185-212, Aug. 2018.   [Online].   Available:
http://futureenergysp.com/index.php/tre/article/view/77/pdf

[14]   M. H. Rehmani, M. Reisslein, A. Rachedi, M. Erol-Kantarci, and M. Radenkovic, "Integrating renewable energy resources into the smart grid: recent developments in information and communication technologies," *IEEE Transactions on Industrial Informatics*, vol. 14, no. 7, pp. 2814-2825, 2018.

[15]   F. R. Yu, P. Zhang, W. Xiao, and P. Choudhury, "Communication systems for grid integration of renewable energy resources," *IEEE Network*, vol. 25, no. 5, pp. 22–29, Sep. 2011.

[16]   B. Heile, "Smart grids for green communications [industry perspectives]," *IEEE Wireless Commun.*, vol. 17, no. 3, pp. 4–6, Jun. 2010.

[17]   A. G. Lazaropoulos, "Statistical Broadband over Power Lines Channel Modeling – Part 1: The Theory of the Statistical Hybrid Model," *Progress in Electromagnetics Research C*, vol. 92, pp. 1-16, 2019. [Online]. Available: http://www.jpier.org/PIERC/pierc92/01.19012902.pdf

[18]   A. G. Lazaropoulos, "Statistical Broadband over Power Lines (BPL) Channel Modeling – Part 2: The Numerical Results of the Statistical Hybrid Model," *Progress in Electromagnetics Research C*, vol. 92, pp. 17-30, 2019. [Online]. Available: http://www.jpier.org/PIERC/pierc92/02.19012903.pdf

[19]   A. G. Lazaropoulos, "Underground Distribution BPL Connections with (N + 1)-hop Repeater Systems: A Novel Capacity Mitigation Technique," *Elsevier Computers and Electrical Engineering*, vol. 40, pp. 1813-1826, 2014.

[20]   A. G. Lazaropoulos, "Review and Progress towards the Capacity Boost of Overhead and Underground Medium-Voltage and Low-Voltage Broadband over Power Lines Networks: Cooperative Communications through Two- and Three-Hop Repeater Systems," *ISRN Electronics*, vol. 2013, Article ID 472190, pp. 1-19, 2013. [Online]. Available: http://www.hindawi.com/isrn/electronics/aip/472190/

[21]   A. G. Lazaropoulos, "Broadband over Power Lines (BPL) Systems Convergence: Multiple-Input Multiple-Output (MIMO) Communications Analysis of Overhead and Underground Low-Voltage and Medium-Voltage BPL Networks (Invited Paper)," *ISRN Power Engineering*, vol. 2013, Article ID 517940, pp. 1-30, 2013. [Online]. Available: http://www.hindawi.com/isrn/power.engineering/2013/517940/

[22]   A. Nazem and M. R Arshad, "An Approach in Full Duplex Digital Multipoint Systems Using Large Signal Power Line Communication," *Bentham Recent Patents on Electrical & Electronic Engineering*, vol. 6, no. 2, pp. 138-146, 2013.

[23]   A. G. Lazaropoulos and P. G. Cottis, "Transmission characteristics of overhead medium voltage power line communication channels," *IEEE Trans. Power Del.*, vol. 24, no. 3, pp. 1164-1173, Jul. 2009.

[24]   A. G. Lazaropoulos and P. G. Cottis, "Capacity of overhead medium voltage power line communication channels," *IEEE Trans. Power Del.*, vol. 25, no. 2, pp. 723-733, Apr. 2010.

[25]   A. G. Lazaropoulos and P. G. Cottis, "Broadband transmission via underground medium-voltage power lines-Part I: transmission characteristics," *IEEE Trans. Power Del.*, vol. 25, no. 4, pp. 2414-2424, Oct. 2010.

[26]   A. G. Lazaropoulos and P. G. Cottis, "Broadband transmission via underground medium-voltage power lines-Part II: capacity," *IEEE Trans. Power Del.*, vol. 25, no. 4, pp. 2425-2434, Oct. 2010.

[27]   A. G. Lazaropoulos, "Broadband transmission and statistical performance properties of overhead high-voltage transmission networks," *Hindawi Journal of Computer Networks and Commun.*, 2012, article ID 875632, 2012. [Online]. Available: http://www.hindawi.com/journals/jcnc/aip/875632/

[28]   A. S. de Beer, A. Sheri, H. C. Ferreira, and A. H. Vinck, "Channel frequency response for a low voltage indoor cable up to 1GHz," In *Power Line Communications and its Applications (ISPLC), 2018 IEEE International Symposium on*, pp. 1-6, 2018.

[29]   A. G. Lazaropoulos, "Enhancing the Statistical Hybrid Model Performance in Overhead and Underground Medium Voltage Broadband over Power Lines Channels by Adopting Empirical Channel Attenuation Statistical Distribution," *Trends in Renewable Energy*, vol. 5, no. 2, pp. 181-217, 2019. [Online]. Available: http://futureenergysp.com/index.php/tre/article/view/96/pdf

[30]   A. G. Lazaropoulos, "Towards Modal Integration of Overhead and Underground Low-Voltage and Medium-Voltage Power Line Communication Channels in the Smart Grid Landscape: Model Expansion, Broadband Signal Transmission Characteristics, and Statistical Performance Metrics (Invited Paper)," *ISRN Signal Processing*, vol. 2012, Article ID 121628, pp. 1-17, 2012. [Online]. Available: http://www.hindawi.com/isrn/sp/2012/121628/

[31]   P. Amirshahi and M. Kavehrad, "High-frequency characteristics of overhead multiconductor power lines for broadband communications," *IEEE J. Sel. Areas Commun.*, vol. 24, no. 7, pp. 1292-1303, Jul. 2006.

[32]   T. Sartenaer, "Multiuser communications over frequency selective wired channels and applications to the powerline access network" *Ph.D. dissertation*, Univ. Catholique Louvain, Louvain-la-Neuve, Belgium, Sep. 2004.

[33]   T. Calliacoudas and F. Issa, ""Multiconductor transmission lines and cables solver," An efficient simulation tool for plc channel networks development," presented at the *IEEE Int. Conf. Power Line Communications and Its Applications*, Athens, Greece, Mar. 2002.

[34]   T. Sartenaer and P. Delogne, "Deterministic modelling of the (Shielded) outdoor powerline channel based on the multiconductor transmission line equations," *IEEE J. Sel. Areas Commun.*, vol. 24, no. 7, pp. 1277-1291, Jul. 2006.

[35]   A. G. Lazaropoulos, "Virtual Indicative Broadband over Power Lines Topologies for Respective Subclasses by Adjusting Channel Attenuation Statistical Distribution Parameters of Statistical Hybrid Models – Part 2: Numerical Results for the Overhead and Underground Medium-Voltage Power Grids," *Trends in Renewable Energy*, vol. 5, no. 3, pp 258-281, Aug. 2019. DOI: 10.17737/tre.2019.5.3.00100

[36]   A. G. Lazaropoulos, "Virtual Indicative Broadband over Power Lines Topologies for Respective Subclasses by Adjusting Channel Attenuation Statistical Distribution Parameters of Statistical Hybrid Models – Part 3: The Case of Overhead Transmission Power Grids," *Trends in Renewable Energy*, vol. 5, no. 3, pp 282-306, Aug. 2019. DOI: 10.17737/tre.2019.5.3.00101

[37]   Matlabtricks (2014) Generate random numbers with a given distribution, http://matlabtricks.com/post-44/generate-random-numbers-with-a-given-distribution (accessed on 8/14/2019)

[38]   J. Denker (2008) Randomly Generating Numbers with an Arbitrary Distribution http://www.av8n.com/physics/arbitrary-probability.htm (accessed on 8/14/2019)